PCCP

Accepted Manuscript

ROYAL SOCIETY OF CHEMISTRY

www.rsc.org/pccp

Free Energy of Solvation of Carbon Nanotubes in the Pyridinium-Based Ionic Liquids

Vitaly V. Chaban and Eudes Eterno Fileti

Instituto de Ciência e Tecnologia, Universidade Federal de São Paulo, 12247-014, São José dos Campos, SP, Brazil

Abstract. Numerous prospective applications require individual carbon nanotubes (CNTs) to be available. Pristine CNTs, strongly hydrophobic by nature, are known to be either totally insoluble or poorly dispersible. While it is unlikely possible to prepare a real solution of CNTs in any solvent, an ability of certain solvents to maintain dispersions of CNTs during macroscopic times constitutes a great research interest. In the present work, we characterize two pyridinium-based ionic liquids (ILs), N-butylpyridinium chloride [BPY][Cl] and N-butylpyridinium bis(trifluoromethanesulfonyl)imide [BPY][TFSI], with respect to their potential to solvate CNTs of different diameter, from CNT (10,10) to CNT (25,25). Using a universal methodology, we found that both ILs exhibit essentially the same solvation performance. Solvation of CNTs is strongly prohibited entropically, whereas the energy penalty increases monotonically with the CNT diameter. Weak van der Waals interactions, which guide enthalpy alteration upon the CNT solvation, are unable to compensate for a large entropic penalty for the ruination of the IL-IL electrostatic interactions. Structure of ILs inside and outside CNTs is also discussed. The reported results are necessary for fundamental understanding of the CNT solvation problematic inspiring search for more suitable solvents.

Key words: carbon nanotube; ionic liquid; pyridinium; solvation free energy.

TOC Image

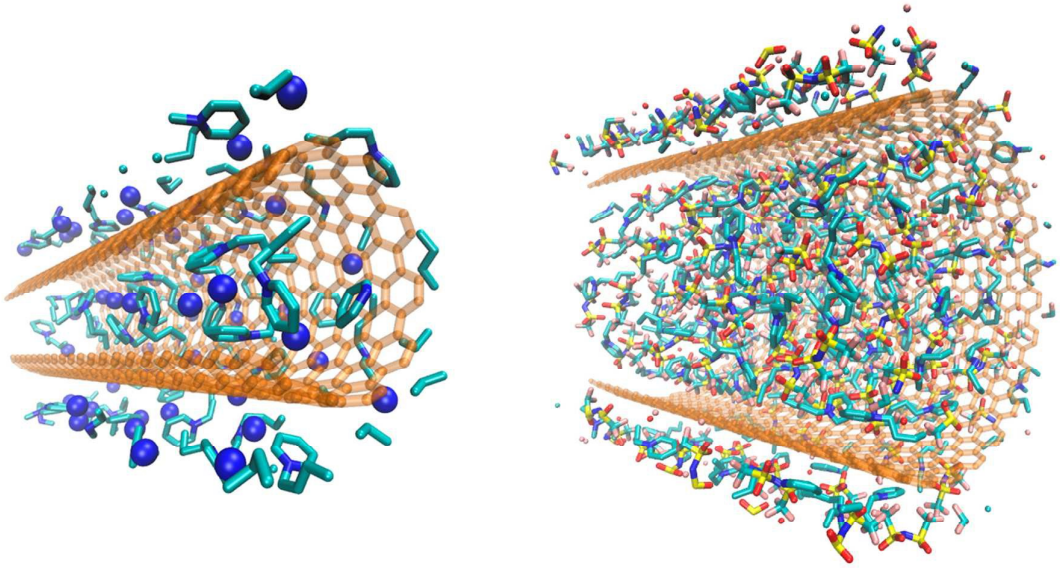

Introduction

Carbon nanotubes (CNTs) constitute a novel class of nanomaterials with remarkable prospective applications in diverse domains. Large surface area, good chemical stability, and a set of exceptional physical properties attract attention of researchers to CNTs during the last two decades.[1-11] CNTs are known to be insoluble or poorly soluble, irrespective of the solvent applied, even though the CNT-CNT non-covalent interactions are fairly weak. In most cases, only the conventional carbon-carbon van der Waals forces were identified. Many theoretically identified device applications require manipulations with the individual CNTs to obtain outstanding productivity.[12-16] Similarly, a proper investigation of CNT chemistry at the molecular level is partially inaccessible without engineering a real solution of pristine CNTs.

Poor solubility originates, first of all, from the size difference of CNTs and liquid molecules. Solvated CNT disturbs genuine structures of the solvents, which results in a significant entropic penalty, which cannot be compensated by the enthalpy gain, thanks to the CNT-solvent attraction. Based on the thermodynamic considerations, the solubility of CNT in any solvent is inversely proportional to its diameter and length. While real solutions of CNTs cannot be thermodynamically favored, some methods were empirically devised to obtain dispersions. For instance, surfactant – such as sodium dodecyl sulfate, sodium cholate etc – and amphiphilic biopolymers, so-called dispersing agents, can be useful.[17] Horn sonication allows for obtaining dispersions of CNTs in chloroform, dimethylformamide, acetone, ethylene glycol, and even methanol by fostering exfoliation of the CNT bundles.[18, 19] Search for better solvents to bring CNTs to the liquid phase in underway during a long time, since many prospective applications will benefit from that.

Ionic liquids (ILs) comprise the most versatile and most vigorously researched class of solvents. The physical chemical properties of ILs can be fine tuned by grouping

different cations and anions and grafting required functional groups to both of them.[20-23] ILs are generally non-volatile, non-flammable, thermally stable, with significant ionic conductivity, gas capture potential, and ability to solvate both hydrophilic and hydrophobic solutes. The practical applications of ILs are actively explored ranging from biphasic systems to electrolyte solutions. Tunability of ILs promises to offer a separate solvent for every application allowing to partially or completely avoid using toxic organic solvents.[21]

ILs may constitute certain interest to dissolve CNTs.[24-26] First, ILs possess hydrophobic moieties, which are expected to coordinate CNTs. Second, aromatic rings of ILs may interact with the sidewalls of CNTs relatively strongly via π-stacking. Third, since ions of ILs are generally larger and more asymmetric than molecules of conventional solvents, the solvent structure perturbations caused by solvation may be less drastic. Fourth, ILs readily penetrate CNTs, while exhibiting strong electrostatic IL-IL interactions. Attraction of the ions inside CNT to the ions outside CNT fosters solubilization.

Several works were published in recent years aiming to investigate CNT-IL physical interactions and their effect on CNT properties.[25, 27-31] Ohba and coworkers[29] used XRD experiments and molecular dynamics (MD) simulations to find structure of a viscous IL, 1-ethyl-3-methylimidazolium chloride, inside CNTs. In narrow CNTs, the anions appear much more movable, as compared to the cations.[30] Another recent work demonstrated that self-diffusion of 1-ethyl-3-methylimidazolium chloride greatly depends on the confinement inside CNTs and on the CNT diameter.[32] The computational predictions were confirmed in the experiments two years later.[33] Aparicio and coworkers[34] investigated interactions of the amino acid ionic liquid with carbon nanostructures. It was found that ion-ionic attraction weakens significantly due to spatial confinement. In turn, the CNT-IL interaction energy increases. The self-diffusion of the IL inside the CNT exceeds that in the bulk phase.

Fukushima and coworkers[35] reported a gel containing CNT and IL, which is stable at room temperature. Raman and IR measurements on the mixtures of ionic liquids and SWCNTs has been shown that no strong interaction such as cation-π interaction exists between SWCNTs and imidazolium ions.[36] Formation of gel is driven by weak van der Waals forces.[36] In turn, Shim and Kim considered solvation of CNT by 1-butyl-3-methylimidazolium tetrafluoroborate.[26] Having obtained encouraging results, they ascribed them largely to π-stacking of the CNT sidewalls and the imidazole rings of the cations.

In the present work, we systematically characterize the potential of pyridinium-based ILs to dissolve CNTs of different curvature. Using MD simulations, CNT solvation is characterized in terms of solvation free energy, which is the most fundamental descriptor that can be derived from atomistic simulations nowadays. N-butylpyridinium chloride, [BPY][Cl], and N-butylpyridinium bis(trifluoromethanesulfonyl)imide, [BPY][TFSI], were chosen for comparison, due to possessing very different anions and different genuine structures.[37] The pyridinium-based ILs were chosen because of having a strongly delocalized charge density over the ring and a hydrophobic moiety (hydrocarbon chain). Furthermore, the pyridinium-based ILs are presently readily available being under vigorous investigation in view of versatile applications.

Methodology

CNTs (10,10), (15,15), (20,20), (25,25), with a length of 5 nm, were placed at the center of the MD cell and surrounded by ILs – [BPY][Cl] and [BPY][TFSI] – to prevent CNT-CNT interactions in view of the periodic images (Table 1). The MD simulations were subsequently performed in the constant temperature constant pressure ensemble to obtain equilibrated configurations (Figure 1).

Table 1. List of the MD systems investigated using classical molecular dynamics simulations to obtain solvation free energies and selected structure properties. Sampling time represents a total time, which was simulated for a given system.

#	Nanotube	# carbon atoms	# ion pairs	# sites	Sampling time, ns
		Nanotubes immersed in [BPY][Cl]			
1	(10,10)	840	250	7090	260
2	(15,15)	1260	350	10010	260
3	(20,20)	1690	500	14180	300
4	(25,25)	2100	700	19600	300
		Nanotubes immersed in [BPY][TFSI]			
5	(10,10)	840	120	5520	220
6	(15,15)	1260	150	7110	220
7	(20,20)	1690	240	11040	300
8	(25,25)	2100	350	15700	300

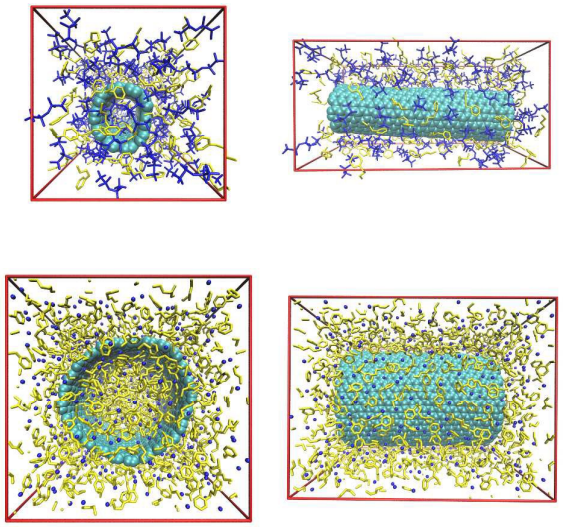

Figure 1. Configurations of the solvated CNTs in the equilibrated MD cells. (Left) Frontal view. (Right) Side view. (Top) CNT (10,10) solvated in [BPY][TFSI]. (Bottom) CNT (25,25) solvated in [BPY][Cl]. The center-of-mass of CNT is forced to coincide with the geometric center of the MD cell during an entire MD simulation. Cations are yellow, anions are blue, CNTs are cyan. The effects due to periodic boundary conditions, such as "broken particles", were removed prior to visualization.

Constant temperature of the MD cell, 350 K, was maintained by the velocity rescaling thermostat[38] with a relaxation time of 0.5 ps. An elevated temperature was simulated to enhance phase space sampling in the high-viscosity environment. Constant pressure, 1 bar, was maintained by the Parrinello-Rahman barostat[39] with a relaxation time of 4.0 ps and a compressibility constant of 4.5×10^{-5} bar^{-1}. The integration time-step of 2.0 fs was used, whereas the carbon-hydrogen covalent bond lengths were kept frozen.[40] Intermediate coordinates and thermodynamic quantities were saved every 5 ps.

The ILs, [BPY][Cl] and [BPY][TFSI], were simulated by means of the recently developed force field,[37] which correctly predicts transport properties and room and somewhat elevated temperatures. CNTs were simulated as a flexible, non-polarizable, non-charged assembly of carbon atoms, linked by harmonic potentials with the following equilibrium values of the bonded parameters: r (C-C)=1.42 nm, A (C-C-C)=120°, D (C-C-C-C)=0°. The intermolecular interaction parameters of the sp^2 carbon were set as σ=0.33 nm, ε=0.41 kJ mol^{-1}. The CNT-IL interaction is exclusively of van der Waals nature, simulated by the Lennard-Jones (12,6) potential. The Lennard-Jones (12,6) interactions were smoothly brought to zero between 1.2 and 1.3 nm using the shifted force technique. The electrostatic interactions were simulated by the Coulomb law for distances below 1.3 nm and using Particle-Mesh-Ewald method[41] for larger distances.

The solvation free energy was computed by the Bennett Acceptance Ratio (BAR) method[42] following step-wise alchemical transformations. A gradual decoupling of the solute molecule from its equilibrium environment was performed by 21 steps: $0 < \lambda < 1$, $\Delta\lambda = 0.05$. With every λ, the system was equilibrated using stochastic dynamics during 3.0 ns. The average $\langle\frac{\partial H(\lambda)}{\partial\lambda}\rangle_\lambda$ was derived from the production trajectory part, ca. 10 ns. Preliminary calculations were used to identify reliable sampling duration at given

temperature and pressure. Lennard-Jones (12,6) and electrostatic interactions were scaled separately.

All reported MD simulations were performed in GROMACS 5.[43, 44] The starting configurations were prepared in PACKMOL.[45] The trajectories of the MD systems were visualized in VMD (Visual Molecular Dynamics, version 1.9.1).[46]

Results and Discussion

Structure of the pyridinium-based ILs in the direction perpendicular to the CNT axis is characterized in Figures 2-3, in terms of the number density distribution functions. A few peaks corresponding to the centers-of-mass of the cation and the anion indicate layered structures of the confined ILs. The observed layers are not regular. Therefore, the confined ILs remain in the liquid state, irrespective of the CNT diameter. In the case of [BPY][Cl], the chloride anions exhibit a larger number of maxima, as compared to $[BPY]^+$. No peaks of significant size were detected in the vicinity of the CNT inner sidewall. The structuring role of CNT is, therefore, relatively modest.

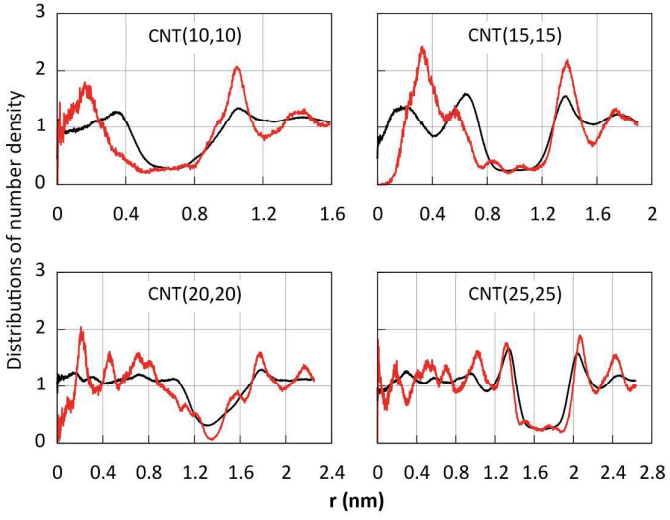

Figure 2. Distributions of number densities of the centers-of-mass of the ions along the normal direction to the CNT axis in [BPY][Cl]. r=0 designates points on the CNT rotation

axis. The minima in the solvent density between 0.8nm and 1.6nm (depending on the NTC) indicates the position of the sidewall of the CNT. The centers-of-mass were computed for the cations (black line) and the anions (red line) separately. See legend for designation of systems.

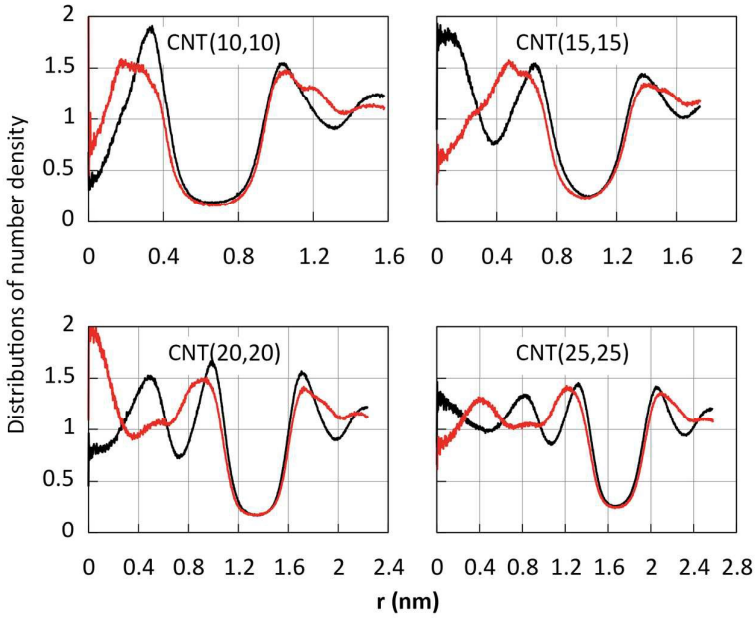

Figure 3. Distributions of number densities of the centers-of-mass of the ions along the normal direction to the CNT axis in [BPY][TFSI]. r=0 designates points on the CNT rotation axis. The minima in the solvent density between 0.8nm and 1.6nm (depending on the NTC) indicates the position of the sidewall of the CNT. The centers-of-mass were computed for the cations (black line) and the anions (red line) separately. See legend for designation of systems.

The number of confined ions inside each CNT is directly proportional to the CNT inner volume (Table 2). Based on the equilibrated snapshots (Figure 1), ILs readily penetrate CNT maintaining density close to that of the corresponding bulk phase, with a correction to boundary conditions (CNT edges). The packing coefficients of the all systems are between 52% (for [BPY][CL] inside CNT (10,10)) and 65% (for [BPY][CL] inside CNT (25,25)), which are in good agreement with the ideal packing coefficient by Rebek's rule that suggests the optimal range of 46-64%.[47]

The ions were allowed to enter and escape CNTs during an entire sampling simulation time (Table 1). Interestingly, CNTs containing [BPY][Cl] inside, appear systematically positively charged. An electron deficiency is implemented thanks to a larger density of $[BPY]^+$. The difference of the number densities of $[BPY]^+$ and $[Cl]^-$ decreases gradually, as the CNT diameter increases. Certain difference still remains inside CNT (25,25), which is close to the stability limit for single-walled CNTs. We suppose that longer CNTs are able to support even larger charge of the confined media. This possibility to generate charge by means of ILs containing different sizes of ions may have interesting practical applications in the field of electrochemistry, where CNT is employed as an electrode.

In the case of [BPY][TFSI], the fractions of the confined cations and anions are within the computed error bars. The density of $[BPY]^+$ within the same CNT depends greatly on the anion. Compare, 42.4 cations of [BPY][Cl] penetrate inside CNT (15,15), whereas only 24.7 cations of [BPY][TFSI] are observed inside the same CNT. Therefore, the density of certain species inside CNTs can be modulated by changing the size of the counter-ion.

Table 2. Average numbers of the cations and the anions inside CNTs. The error bars were computed based on the statistical processing of a large number of system snapshots along the entire simulation trajectory. Upon analysis, an ion was ascribed to the inside region only when all of its atoms belonged to the cylindrical cavity inside CNT.

CNT	[BPY][Cl]		[BPY][TFSI]	
	# cations	# anions	# cations	# anions
(10,10)	13.2 ± 0.4	9.0 ± 0.2	9.0 ± 0.3	8.3 ± 0.5
(15,15)	42.4 ± 0.5	36.1 ± 0.4	24.7 ± 1.1	22.8 ± 0.9
(20,20)	85.2 ± 1.4	77.8 ± 1.1	46.2 ± 1.2	47.0 ± 1.0
(25,25)	142.6 ± 1.5	141.0 ± 1.4	77.5 ± 1.5	74.3 ± 1.4

Solvation shell of CNT (a hydrophobic solute) is poorly defined, but can still be distinguished. The centers-of-mass of the first shell of the outside ions are located 5-7 Å away from the outer surface of CNTs. We did not find any dependence of this value on the CNT curvature, probably because the boundaries of the shell are relatively smashed. Figure 4 depicts solvation shells of a few CNTs along with the confined ions. The CNTs remain completely filled during the MD simulations. Furthermore, the outer shell of solvent can be observed comprising both cations and anions. No preferential coordination of CNT by any of the ions was observed, although one may expect that the pyridine ring exhibits a higher affinity to the CNT thanks to π-stacking.

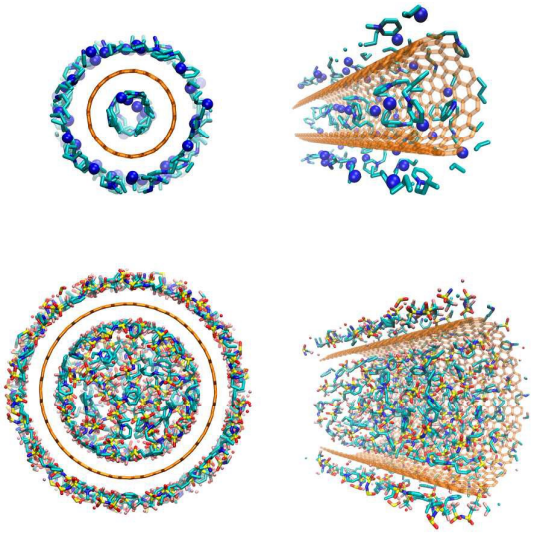

Figure 4. Immediate structures of the first solvation shells. (Top) CNT (10,10) in [BPY][Cl]; (bottom) CNT (25,25) in [BPY][TFSI]. The thickness of the CNT sidewall was set to hairline for visualization purposes. Chloride anions are blue balls, N-butylpyridinium cations are cyan sticks, carbon atoms of CNTs are orange sticks.

CNT filling by ionic and molecular liquids is determined by two easily measurable physical properties: surface tension of the pure liquid, which is expected to fill out the CNT, and CNT–liquid attraction. Surface tension of most liquids is experimentally known. In turn, the CNT–liquid attraction can be obtained from computer simulations using ab

initio methods to parametrize atom-atom interactions and molecular mechanics to efficiently consider large atomic ensembles.

Figure 5 depicts CNT-cation and CNT-anion interaction energies versus the CNT curvature. The interaction energies were obtained by averaging out immediate energies along the MD trajectory. Since it is obvious that a larger object exhibits a higher interaction energy associated with it, all energies were normalized with respect to carbon atoms belonging to the respective CNT. Interestingly, nearly no systematic dependence on the CNT size was found. In turn, different ions exhibit different interaction energies with CNTs. Both inside and outside ions were included in the present analysis.

The strongest interaction occurs between CNTs and $[BPY]^+$ in [BPY][Cl], ranging between -5.3 and -5.5 kJ mol^{-1}. In turn, the weakest interaction takes place in the case of chloride, ca. -0.6 kJ mol^{-1}. Despite interesting effects caused by chloride, as discussed above, this anion is not useful for dispersing CNTs in ILs. The performance of BPY^+ and $TFSI^-$ in [BPY][TFSI] is nearly the same. Note the different CNT-$[BPY]^+$ contributions in [BPY][Cl] and [BPY][TFSI]. Inside CNT (10,10), $TFSI^-$ interacts more strongly, -3.9 kJ mol^{-1}, since this ion is more flexible. It appears more successful to approach the high-curvature surface of CNT (10,10). On the contrary, the aromatic pyridine ring is essentially rigid.

Unlike electronic-structure methods, MD simulations constitute an inherently suitable tool to decompose potential energy into multiple components. Although one must keep in mind that additivity of intermolecular interactions is a simplification of their real nature, it allows for straightforward deciphering of a role of each component in the total solvation energy.

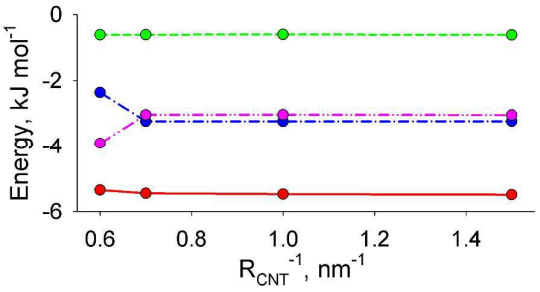

Figure 5. Decomposition of the non-covalent energy into pairwise contributions as a function of the CNT curvature. In [BPY][Cl]: CNT-$[BPY]^+$ (red solid line), CNT-$[Cl]^-$ (green dashed line). In [BPY][TFSI]: CNT-$[BPY]^+$ (blue dash-dotted line), CNT-$[TFSI]^-$ (pink dash-dot-dotted line). The error bars are smaller than the radius of the depicted symbols.

Solvation free energy is the most fundament property, which can be related to solubility in the approximation of an ideal behavior. Free energy comprises two components: enthalpic factor (ΔH) and entropic factor ($T\Delta S$), $\Delta G=\Delta H - T\Delta S$. The enthalpic factor is naturally negative, originating from the attractive solvent-solute interactions. For a good solubility to be attained, it must be maximized by selecting the most appropriate cations and anions and performing their task-specific functionalization. The entropic factor is proportional to temperature and depends on a large variety of the structure-related features. If the solute ruins peculiar interactions in the solvent, such as hydrogen-bonded networks, the result is a big entropic penalty, $T\Delta S << 0$. If the solute fosters solvent rearrangement in a more energetically efficient manner than it is in the pure liquid, the entropic factor will be favorable, $T\Delta S > 0$.

Figure 6 depicts the enthalpic factor and the entropic factor as a function of the CNT curvature. Both factors depend on the curvature significantly. Solvation of CNT in the pyridinium-based ILs is moderately favored by enthalpy and strongly prohibited by entropy. Herewith, wider CNTs exhibit more negative ΔH, but also more positive $-T\Delta S$. Larger CNTs introduce larger perturbations of the bulk IL structure. In the meantime, penetration of the solvents into wider CNTs is naturally easier. [BPY][TFSI] performs

better in enthalpy, but worse in entropy. In the case of CNT (10,10), the difference is within the computed error bars.

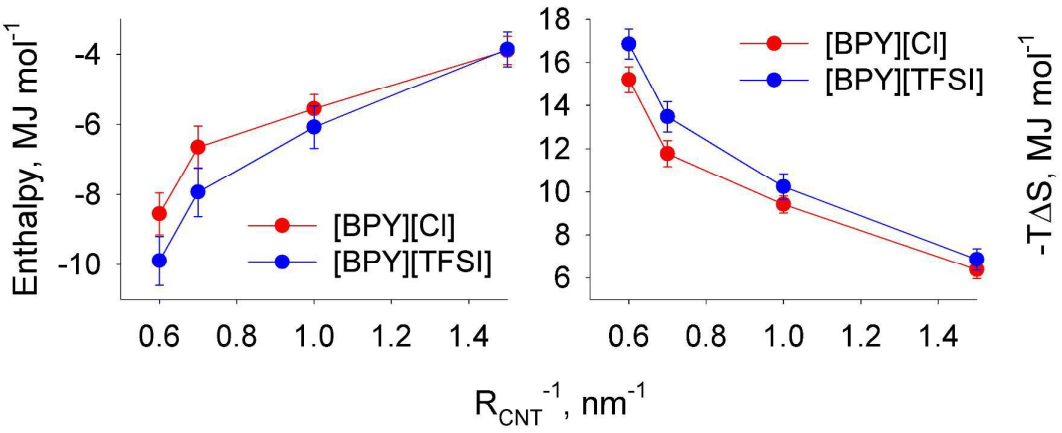

Figure 6. Enthalpic (left) and entropic (right) factors determining solvation of CNTs (10,10), (15,15), (20,20), and (25,25) in [BPY][Cl] (red circles) and [BPY][TFSI] (blue circles) and 350 K and 1 bar.

The average free energy of solvation appears significantly positive (Figure 7), irrespective of the CNT used. Thus, the results of the computations confirm a poor solubility of CNTs. Wider CNTs are systematically less soluble. While ΔG=+2.5 MJ mol^{-1} for CNT (10,10) in [BPY][Cl], ΔG=+6.6 MJ mol^{-1} for CNT (25,25) in the same solvent. An average ΔG in [BPY][Cl] is slightly smaller than that in [BPY][TFSI], but the values fall within the error bars of the present simulations. The error bars must be decreased by increasing sampling to make the observed difference statistically meaningful.

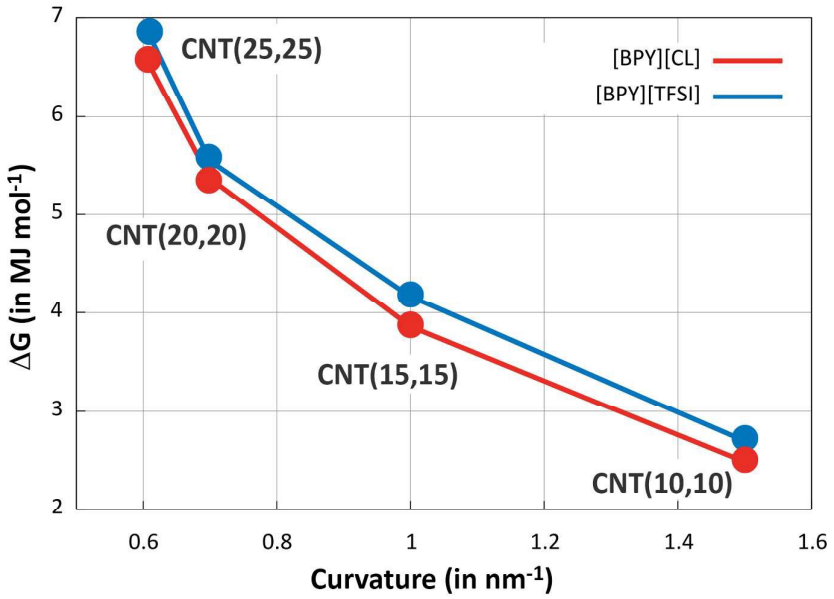

Figure 7. Solvation free energy of CNTs (10,10), (15,15), (20,20), and (25,25) in [BPY][Cl] (red circles) and [BPY][TFSI] (blue circles) as a function of CNT curvature. The size of the symbols is comparable with the computed error bars.

The present work considers CNTs of finite length. If the CNT length is changed, the computed thermodynamic quantities must be rescaled linearly. However, if the CNT diameter is adjusted, an extrapolation is not straightforward. An effect of the CNT diameter is specific to each IL, since structure perturbations due to solvation depend on the size of ions and ionic clusters, which exist in the particular IL. Table 3 shows thermodynamic potentials per mole of carbon atoms of CNTs to compare different CNTs to one another. Apparently, an effect of the CNT curvature disappears, ΔG ranges from 3.0 to 3.2 kJ mol^{-1} the difference being within error bars for all CNTs. Despite this interesting result, one must use non-normalized values in all thermodynamic transformations. For instance, to assess solubilities of CNTs, the following equation can be employed, $K = \exp(-\Delta G/RT)$, where ΔG must correspond to a mole of CNTs.

Table 3. Free energies, enthalpies and entropies per one mole of the CNT carbon atoms for solvation of CNTs in [BPY][Cl] and [BPY][TFSI].

CNT	ΔG, kJ mol^{-1}	ΔH, kJ mol^{-1}	-TΔS, kJ mol^{-1}

[BPY][Cl]			
(10,10)	3.0 ± 0.1	-4.6 ± 0.4	7.6 ± 0.5
(15,15)	3.1 ± 0.1	-4.4 ± 0.4	7.5 ± 0.5
(20,20)	3.2 ± 0.1	-4.2 ± 0.4	7.4 ± 0.5
(25,25)	3.2 ± 0.1	-4.1 ± 0.4	7.2 ± 0.5
[BPY][TFSI]			
(10,10)	3.2 ± 0.1	-4.6 ±0.4	7.8 ± 0.5
(15,15)	3.3 ± 0.1	-4.8 ±0.4	8.1 ± 0.5
(20,20)	3.3 ± 0.1	-4.7 ±0.4	8.0 ± 0.5
(25,25)	3.3 ± 0.1	-4.7 ±0.4	8.0 ± 0.5

Conclusions

Classical molecules dynamics simulations were carried out for solvation of CNTs (10,10), (15,15), (20,20), and (25,25) in [BPY][Cl] and [BPY][TFSI]. Solvation free energies, solvation enthalpies, and solvation entropies were computed based on the extensive sampling of the phase space at 350 K and 1 bar. The structures of ILs were described inside and outside all CNTs.

Free energies of solvation of CNTs in [BPY][Cl] and [BPY][TFSI] were found to be significantly positive. Accordingly, solubility of CNTs in ILs is very modest. Solvation of CNT (10,10) is clearly more thermodynamically favorable than solvation of CNT (25,25). This is a result of larger perturbations of the IL structure introduced by large CNTs. Although the enthalpy alteration is negative (favorable for dissolution), it is unable to properly compensate for the above discussed entropic penalty. Functionalization of CNTs with hydrophilic groups is definitely helpful to enhance their interactions with polar solvents, such as ILs. Despite different genuine structures of the investigated ILs, their performance with respect to the CNT solvation is essentially the same. This result is quite insightful being poorly predictable.

The applied methodology of simulations is universal in the sense that it does not depend on the simulations setup, but is determined by exclusively interactions of CNTs

and ILs. The pyridinium-based ILs can be substituted by other ionic and molecular liquids. The solvation free energies obtained in such simulations can be directly compared to one another. One must, of course, keep in mind that the formula connecting solvation free energy and solubility at given temperature and pressure assumes an ideal behavior. Furthermore, thermodynamic properties characterize only the difference between the beginning state and the end state, while ignoring the process itself. Energy barriers may occur along the solubilization pathway, thereby introducing some corrections to the predicted solubilities. Despite having a negative free energy change, certain processes (especially, chemical reactions) may be kinetically forbidden.

Acknowledgments

Partial support was obtained from FAPESP, CAPES, and CNPq.

References

1. A. B. Kaiser and V. Skakalova, *Chemical Society Reviews*, 2011, 40, 3786-3801.
2. L. B. Hu, D. S. Hecht and G. Gruner, *Chemical Reviews*, 2010, 110, 5790-5844.
3. A. C. Dillon, *Chemical Reviews*, 2010, 110, 6856-6872.
4. P. A. Denis, F. Iribarne and R. Faccio, *J Chem Phys*, 2009, 130.
5. R. Chapman, M. Danial, M. L. Koh, K. A. Jolliffe and S. Perrier, *Chemical Society Reviews*, 2012, 41, 6023-6041.
6. A. M. Caminade and J. P. Majoral, *Chemical Society Reviews*, 2010, 39, 2034-2047.
7. P. A. Denis, *J Phys Chem C*, 2011, 115, 20282-20288.
8. T. G. Barclay, K. Constantopoulos and J. Matisons, *Chemical Reviews*, 2014, 114, 10217-10291.
9. R. Long, *Journal of Physical Chemistry Letters*, 2013, 4, 1340-1346.
10. M. Adeli, R. Soleyman, Z. Beiranvand and F. Madani, *Chemical Society Reviews*, 2013, 42, 5231-5256.
11. R. Long and O. V. Prezhdo, *Nano Letters*, 2014, 14, 3335-3341.
12. O. Amelines-Sarria, V. A. Basiuk, V. Duarte-Alaniz and M. Rivera, *Physical Chemistry Chemical Physics*, 2015, 17, 27399-27408.
13. M. S. Dresselhaus, *Acs Nano*, 2010, 4, 4344-4349.
14. M. Bansal, R. Srivastava, C. Lal, M. N. Kamalasanan and L. S. Tanwar, *Nanoscale*, 2009, 1, 317-330.

15. V. A. Basiuk and L. V. Henao-Holguin, *Journal of Computational and Theoretical Nanoscience*, 2014, 11, 1609-1615.
16. D. Janas and K. K. Koziol, *Nanoscale*, 2014, 6, 3037-3045.
17. P. Angelikopoulos and H. Bock, *Physical Chemistry Chemical Physics*, 2012, 14, 9546-9557.
18. K. Balamurugan, P. Baskar, R. M. Kumar, S. Das and V. Subramanian, *Physical Chemistry Chemical Physics*, 2014, 16, 24509-24518.
19. A. Di Crescenzo, M. Aschi, E. Del Canto, S. Giordani, D. Demurtas and A. Fontana, *Physical Chemistry Chemical Physics*, 2011, 13, 11373-11383.
20. V. V. Chaban and O. V. Prezhdo, *Journal of Physical Chemistry Letters*, 2013, 4, 1423-1431.
21. A. Figoli, T. Marino, S. Simone, E. Di Nicolo, X. M. Li, T. He, S. Tornaghi and E. Drioli, *Green Chemistry*, 2014, 16, 4034-4059.
22. A. Jordan and N. Gathergood, *Chemical Society Reviews*, 2015, 44, 8200-8237.
23. T. Mandai, K. Yoshida, K. Ueno, K. Dokko and M. Watanabe, *Physical Chemistry Chemical Physics*, 2014, 16, 8761-8772.
24. M. Mohammadi and M. Foroutan, *Physical Chemistry Chemical Physics*, 2013, 15, 2482-2494.
25. Z. Q. He and P. Alexandridis, *Physical Chemistry Chemical Physics*, 2015, 17, 18238-18261.
26. Y. Shim and H. J. Kim, *Acs Nano*, 2009, 3, 1693-1702.
27. V. V. Chaban, A. Arruda and E. E. Fileti, *Physical Chemistry Chemical Physics*, 2015, 17, 26386-26393.
28. Y. Y. Jiang, K. Zhang, H. Li, Y. Z. He and X. G. Song, *Nanoscale*, 2012, 4, 7063-7069.
29. T. Ohba and V. V. Chaban, *Journal of Physical Chemistry B*, 2014, 118, 6234-6240.
30. T. Ohba, K. Hata and V. V. Chaban, *Journal of Physical Chemistry C*, 2015, 119, 28424-28429.
31. S. Perkin, *Physical Chemistry Chemical Physics*, 2012, 14, 5052-5062.
32. V. V. Chaban and O. V. Prezhdo, *Acs Nano*, 2014, 8, 8190-8197.
33. Q. Berrod, F. Ferdeghini, P. Judeinstein, N. Genevaz, R. Ramos, A. Fournier, J. Dijon, J. Ollivier, S. Rols, D. Yu, R. A. Mole and J. M. Zanotti, *Nanoscale*, 2016, 8, 7845-7848.
34. C. Herrera, R. Alcalde, G. Garcia, M. Atilhan and S. Aparicio, *Journal of Physical Chemistry C*, 2015, 119, 27080-27094.
35. T. Fukushima, A. Kosaka, Y. Ishimura, T. Yamamoto, T. Takigawa, N. Ishii and T. Aida, *Science*, 2003, 300, 2072-2074.
36. J. Y. Wang, H. B. Chu and Y. Li, *Acs Nano*, 2008, 2, 2540-2546.
37. I. V. Voroshylova and V. V. Chaban, *Journal of Physical Chemistry B*, 2014, 118, 10716-10724.
38. G. Bussi, D. Donadio and M. Parrinello, *J Chem Phys*, 2007, 126, 014101.
39. M. Parrinello and A. Rahman, *J. Appl. Phys.*, 1981, 52, 7182-7192.
40. B. Hess, H. Bekker, H. J. C. Berendsen and J. G. E. M. Fraaije, *J. Comp. Chem.*, 1997, 18, 1463.
41. T. Darden, D. York and L. Pedersen, *J. Chem. Phys.*, 1993, 98, 10089-10099.
42. C. H. Bennett, *Journal of Computational Physics*, 1976, 22, 245-268.
43. E. Lindahl, B. Hess and D. Van Der Spoel, *Journal of Molecular Modeling*, 2001, 7, 306-317.
44. H. J. C. Berendsen, D. Vanderspoel and R. Vandrunen, *Computer Physics Communications*, 1995, 91, 43-56.

45. L. Martinez, R. Andrade, E. G. Birgin and J. M. Martinez, *J Comput Chem*, 2009, 30, 2157-2164.
46. W. Humphrey, A. Dalke and K. Schulten, *Journal of Molecular Graphics*, 1996, 14, 33-38.
47. S. Mecozzi and J. J. Rebek, *Chemistry - A European Journal*, 1998, 4, 1016-1022.